Accurate optical vector network analyzer based on optical single-sideband modulation and balanced photodetection

Min Xue, Shilong Pan,* and Yongjiu Zhao

Key Laboratory of Radar Imaging and Microwave Photonics, Ministry of Education, Nanjing University of Aeronautics and Astronautics, Nanjing 210016, China

**Corresponding author: pans@ieee.org*

Received October 23, 2014; revised January 2, 2015; accepted January 12, 2015; posted January 14, 2015 (Doc. ID 225574); published February 10, 2015

A novel optical vector network analyzer (OVNA) based on optical single-sideband (OSSB) modulation and balanced photodetection is proposed and experimentally demonstrated, which can eliminate the measurement error induced by the high-order sidebands in the OSSB signal. According to the analytical model of the conventional OSSB-based OVNA, if the optical carrier in the OSSB signal is fully suppressed, the measurement result is exactly the high-order-sideband-induced measurement error. By splitting the OSSB signal after the optical device-under-test (ODUT) into two paths, removing the optical carrier in one path, and then detecting the two signals in the two paths using a balanced photodetector (BPD), high-order-sideband-induced measurement error can be ideally eliminated. As a result, accurate responses of the ODUT can be achieved without complex post-signal processing. A proof-of-concept experiment is carried out. The magnitude and phase responses of a fiber Bragg grating (FBG) measured by the proposed OVNA with different modulation indices are superimposed, showing that the high-order-sideband-induced measurement error is effectively removed.

OCIS codes: (300.6320) Spectroscopy, high-resolution; (120.0120) Instrumentation, measurement, and metrology; (060.5625) Radio frequency photonics.

http://dx.doi.org/10.1364/OL.40.000569

Many emerging applications, such as single-molecule detection [1], optical storage based on slow light [2], on-chip nonlinear effects [3], and high-precision optical sensing [4], essentially desire a sharp magnitude or phase change within an ultra-small spectral range. Optical devices with ultra-high quality factor (Q), which have the capability to handle the optical spectra with high fineness, are thus of critical importance. With the continuous efforts devoted to the development of such high-Q devices, the state-of-the-art narrowband fiber Bragg grating (FBG) has a 3-dB bandwidth of 9 MHz [5], and the Q value of the optical micro-resonators can reach 6×10^{10} (corresponding to a 3-dB bandwidth of 3 kHz at 1550 nm) [6]. To achieve the optical magnitude and phase responses of these devices, an optical vector network analyzer (OVNA) with ultra-high resolution is needed. Conventionally, the OVNAs based on modulation phase-shifted method [7] or interferometry approach [8] achieve wavelength sweeping by scanning the wavelength of a laser source. Restricted by the low resolution and poor wavelength stability of the state-of-the-art wavelength-swept laser source, the resolution of these OVNAs is usually larger than 1.6 pm, which is not enough to obtain the accurate spectral responses of the ultrahigh-Q optical devices. To solve this problem, OVNAs based on optical single-sideband (OSSB) modulation were proposed and demonstrated [9–13]. Benefiting from the high-resolution frequency sweeping and accurate magnitude and phase detection in the electrical domain, the resolution of the OSSB-based OVNA can reach several hertz in theory [9] and 78 kHz in experiment [10]. However, the OSSB modulation based on electro-optic modulators (EOMs) always stimulates many high-order sidebands (i.e., $\pm 2^{\text{nd}}$–, $\pm 3^{\text{rd}}$–, …, $\pm n^{\text{th}}$-order sidebands), which would introduce considerable measurement error [11], especially, when the EOMs have large phase modulation indices. Previously, we demonstrated a method to effectively suppress the high-order-sideband-induced measurement error [12] based on a two-step measurement followed by post-signal processing. However, the method is relatively complex and time consuming, which would not be able to measure the optical devices with high-Q value since the their spectral responses are always sensitive to the temperature variation and mechanical vibration.

In this Letter, a novel OSSB-based OVNA with suppression of the high-order-sideband-induced measurement error is proposed and demonstrated based on balanced photodetection. Without complex post-signal processing, accurate optical spectral responses with high resolution can be obtained by only single-step measurement. In the measurement, the OSSB signal, after propagating through an optical device-under-test (ODUT), is divided into two parts. One part is directly sent to one input port of a balanced photodetector (BPD), and the other one is first connected to an optical filter to remove the optical carrier, and then directed to the other input port of the BPD. Letting the length of the two optical paths identical, the two signals are vectorially subtracted in the BPD. According to the analytical model of the OSSB-based OVNA, the detection of the OSSB signal with the optical carrier results in the spectral responses with high-order-sideband-induced measurement error, while the optical single-sideband-suppressed carrier (OSSB-SC) signal can obtain only the high-order-sideband-induced measurement error. As a result, the high-order-sideband-induced measurement error is removed, and the output photocurrent of the BPD carries exactly the responses of the ODUT. A proof-of-concept experiment is performed. The accurate magnitude and phase responses of a FBG are successfully measured by the proposed OVNA. Measurement results are almost identical for OSSB

modulations with different modulation indices. The measured magnitude and phase responses agree well with those measured by a commercial OVNA (LUNA OVA5000).

Figure 1 shows the schematic diagram of the proposed OVNA based on OSSB modulation and balanced photodetection. An optical carrier from a tunable laser source (TLS) is modulated by a RF signal from a RF source at an OSSB modulator, which generates an OSSB signal. Mathematically, the RF modulated OSSB signal after the OSSB modulator can be written as

$$E_{\text{in}}(\omega) = A_0\delta(\omega-\omega_o) + \sum_{\substack{n=-\infty\\ n\neq -1,0}}^{+\infty} A_n\cdot\delta[\omega-(\omega_o+n\omega_e)], \quad (1)$$

where ω_o and ω_e are the angular frequencies of the optical carrier and the RF signal, respectively, and A_n is the complex amplitude of the n^{th}-order sideband.

When the OSSB signal propagates through an ODUT, the magnitude and phase of the optical carrier and sidebands are changed according to the transmission function of the ODUT. Then, an optical splitter divides the optical signal into two parts. One part is directly introduced to one input port of a BPD (the upper path). The other part is directed to the BPD via an optical filter that suppresses the optical carrier (the lower path). The upper and lower paths are adjusted to have the same length. Assuming the optical carrier of the optical signal in the lower path is fully removed, the optical field in the two paths can be expressed as

$$E_U(\omega) = B_0H(\omega_o)\delta(\omega-\omega_o) + \sum_{\substack{n=-\infty\\ n\neq -1,0}}^{+\infty} H(\omega_o+n\omega_e)B_n\cdot\delta[\omega-(\omega_o+n\omega_e)] \quad (2.1)$$

$$E_L(\omega) = \sum_{\substack{n=-\infty\\ n\neq -1,0}}^{+\infty} H(\omega_o+n\omega_e)B_n\cdot\delta[\omega-(\omega_o+n\omega_e)] \quad (2.2)$$

where $H(\omega) = H_{\text{ODUT}}(\omega)\cdot H_{\text{sys}}(\omega)$, and $H_{\text{ODUT}}(\omega)$ and $H_{\text{sys}}(\omega)$ are the transmission functions of the ODUT and measurement system, respectively. B_n is the complex amplitude of the n^{th}-order sideband of the optical signals in these two paths.

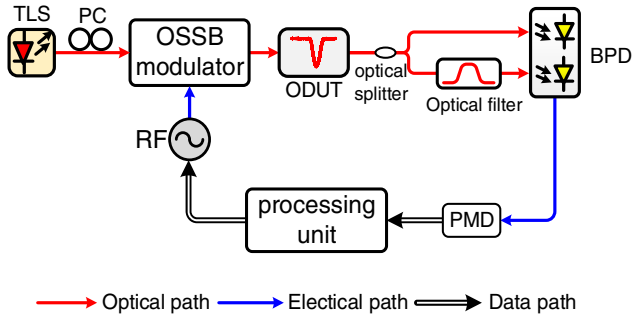

Fig. 1. Schematic diagram of the proposed OVNA based on OSSB modulation and balanced photodetection. TLS: tunable laser source; PC: polarization controller; RF: radio frequency; ODUT: optical device-under-test; BPD: balanced photodetector; PMD: phase-magnitude detector.

In the BPD, the optical signals in the upper and lower paths are simultaneously converted into electrical signals. The ω_e components of the converted signals can be written as

$$i_U(\omega_e) = \frac{\eta}{2\pi}B_1B_0^*H(\omega_o+\omega_e)H^*(\omega_o) + \frac{\eta}{2\pi}\sum_{\substack{n=-\infty\\ n\neq -1,0}}^{\infty} B_{n+1}B_n^*H[\omega_o+(n+1)\omega_e]H^*(\omega_o+n\omega_e) \quad (3.1)$$

$$i_L(\omega_e) = \frac{\eta}{2\pi}\sum_{\substack{n=-\infty\\ n\neq -1,0}}^{\infty} B_{n+1}B_n^*H[\omega_o+(n+1)\omega_e]H^*(\omega_o+n\omega_e), \quad (3.2)$$

where η is the responsivity of the BPD. On the right-hand of Eq. (3.1), the first term represents the spectral responses of the ODUT, and the second term is the high-order-sideband-induced measurement error. Eq. (3.2) is exactly the high-order-sideband-induced measurement error.

At the output port of the BPD, the photocurrents are vectorially subtracted, so the output current of the BPD is

$$i(\omega_e) = i_U(\omega_e) - i_L(\omega_e) = \frac{\eta}{2\pi}B_1B_0^*H(\omega_o+\omega_e)H^*(\omega_o). \quad (4)$$

$H_{\text{sys}}(\omega)$ can be measured by a calibration step in which the ODUT is removed and the two test ports are directly connected, i.e., $H_{\text{ODUT}}(\omega) = 1$. In this case, the transmission function of the measurement system can be acquired which can be expressed as

$$i_{\text{sys}}(\omega_e) = \frac{\eta}{2\pi}B_1B_0^*H_{\text{sys}}(\omega_o+\omega_e)H_{\text{sys}}^*(\omega_o). \quad (5)$$

From Eqs. (4) and (5), the actual spectral responses of the ODUT without the high-order-sideband-induced measurement error can be obtained, given by

$$H_{\text{ODUT}}(\omega_o+\omega_e) = \frac{i(\omega_e)}{i_{\text{sys}}(\omega_e)H_{\text{ODUT}}^*(\omega_o)}, \quad (6)$$

where $H_{\text{ODUT}}^*(\omega_o)$ is a constant since it is the frequency response of the ODUT at a fixed wavelength.

A proof-of-concept experiment based on the setup shown in Fig. 1 is carried out. A lightwave with a power of 16 dBm is generated by a TLS (Agilent N7714A), which is modulated by a RF signal from an electrical vector network analyzer (EVNA, Agilent N5245A) at an OSSB modulator. In the experiment, the OSSB modulator is implemented by a polarization modulator (PolM, Versawave Inc.), a polarization controller (PC), a polarizer (Pol), and an optical filter (Finisar WaveShaper 4000 s) [14]. After propagating through a FBG (TeraXion Inc.), which is used as an ODUT, the OSSB signal is

divided into two parts by an optical splitter. In the upper path, a variable optical delay line and a variable optical attenuator are inserted to balance the optical path and the insertion loss of the two paths, respectively. In the lower path, the optical carrier is removed by a tunable optical filter (Yenista XTM-50). A 50-GHz BPD (U2T BPD2150R) is employed to convert the two optical signals from the two paths to a RF signal, which is then received by a phase-magnitude detector in the EVNA. A wideband RF power amplifier (SHF 806E) is applied to amplify the RF signal from the EVNA to a satisfactory power level. The optical spectra are monitored by an optical spectrum analyzer (Yokogawa AQ6370C) with a resolution of 0.02 nm.

Figure 2 shows the optical spectra of the OSSB signal in the upper path and the OSSB-SC signal in the lower paths when the modulation index is 2.81. As can be seen, the optical carrier of the OSSB signal in the lower path is suppressed by 34.2 dB, while the other sidebands maintain almost the same powers. The optical power of the OSSB signal is 3.44-dB larger than that of the OSSB-SC signal.

Figure 3 shows the magnitude and phase responses of the FBG measured by the conventional and proposed OVNAs with a phase modulation index of 2.81. From Fig. 3, the magnitude and phase responses measured by the conventional OVNA contain considerable high-order-sideband-induced error. However, when the proposed OVNA is applied, the error is significantly reduced. Figure 4 shows the magnitude and phase responses of the FBG measured by the proposed OVNA with different phase modulation indices. As a comparison, the results measured by a commercial OVNA (LUNA OVA5000) are also plotted. As can be seen from Figs. 4(a) and 4(b), the magnitude and phase responses measured by the proposed OVNA with different phase modulation indices are coincident, which agree well with those measured by LUNA OVA5000 [the black solid diamond lines in Figs. 4(a) and 4(b)].

Theoretically, the high-order-sideband-induced error can be completely suppressed by carefully adjusting the lengths and losses of the two paths. However, in practice the influence of the temperature variation on the fiber lengths and the uneven frequency response of the BPD must be considered. Considered that the length of the fibers in the two paths are shorter than 3 m and the temperature variation is smaller than 1°C in the laboratory environment, the RF common mode rejection ratio can keep very large in the experiment, for instance more than 34 dB at 40 GHz. Figure 5 shows the frequency response of the BPD when two identical signals are

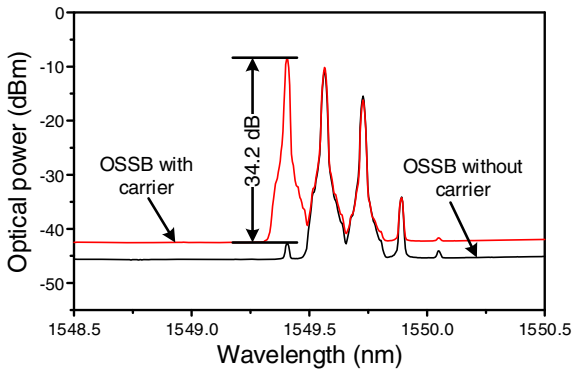

Fig. 2. Optical spectra of the OSSB signal and the OSSB-SC signal with a modulation index of 2.81.

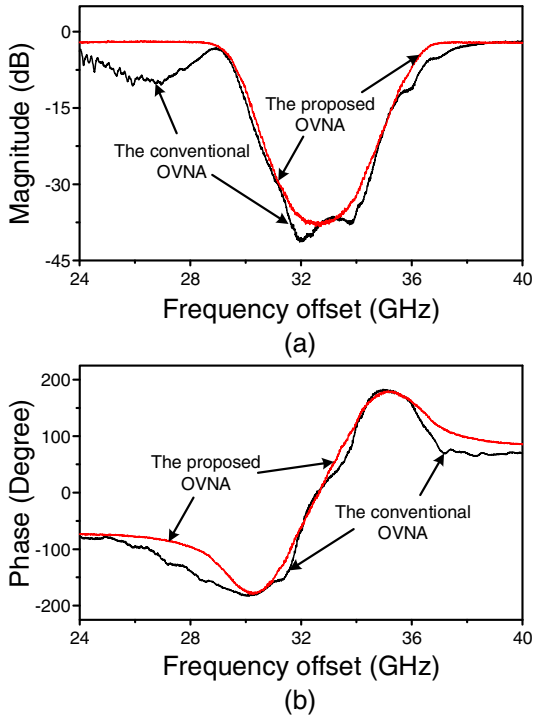

Fig. 3. (a) Magnitude and (b) phase responses measured by the conventional and proposed OVNAs with a modulation index of 2.81.

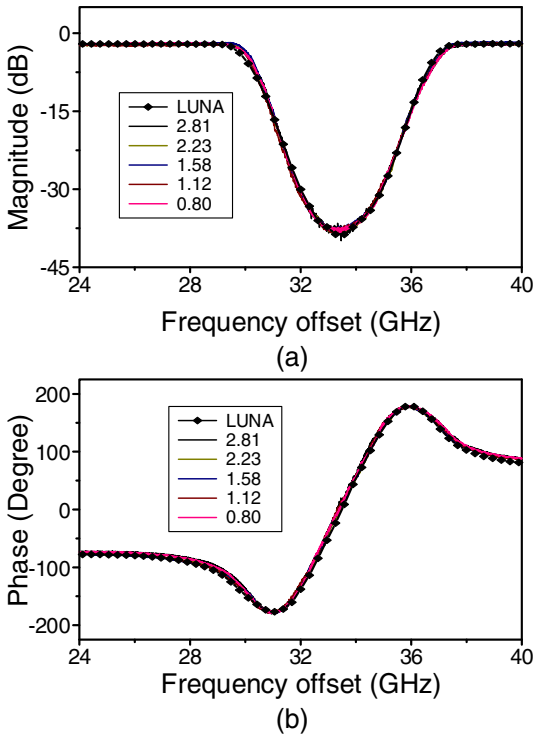

Fig. 4. (a) Magnitude and (b) phase responses measured by the proposed OVNA with different phase modulation indices and a commercial OVNA (LUNA OVA5000).

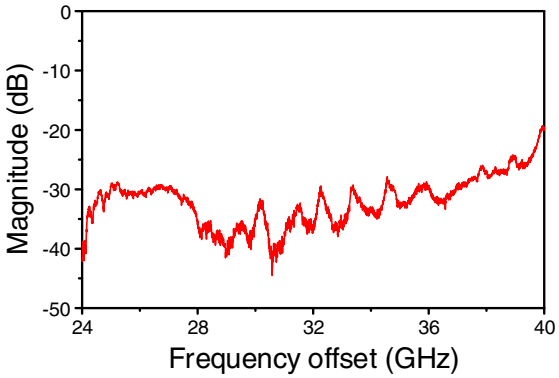

Fig. 5. Frequency response of the BPD when two identical signals are introduced to the two input ports.

introduced to the two input ports. As can be seen, the RF common mode rejection ratio of the BPD is larger than 20 dB, indicating that the high-order-sideband-induced measurement error can be reduced to less than 1%. By using a BPD with smaller imbalance of responsivity, the performance of the system could be further improved.

In conclusion, a novel OSSB-based OVNA with suppressed high-order-sideband-induced measurement error was proposed and experimentally demonstrated using balanced photodetection. In the proof-of-concept experiment, the magnitude and phase responses of a FBG with largely suppressed high-order-sideband-induced measurement error were achieved without any complex post signal processing.

This work was supported in part by the National Natural Science Foundation of China (61422108), the National Basic Research Program of China (2012CB315705), the Jiangsu Provincial Program for High-level Talents in Six Areas (DZXX-034), the Fundamental Research Funds for the Central Universities, Funding of Jiangsu Innovation Program for Graduate Education (CXZZ12_0154), the Funding for Outstanding Doctoral Dissertation in NUAA (BCXJ13-08), and a Project Funded by the Priority Academic Program Development of Jiangsu Higher Education Institutions.

References

1. V. G. Kravets, F. Schedin, R. Jalil, L. Britnell, R. V. Gorbachev, D. Ansell, B. Thackray, K. S. Novoselov, A. K. Geim, A. V. Kabashin, and A. N. Grigorenko, Nat. Mater. **12**, 304 (2013).
2. L. Liu, R. Kumar, K. Huybrechts, T. Spuesens, G. Roelkens, E.-J. Geluk, T. de Vries, P. Regreny, D. Van Thourhout, R. Baets, and G. Morthier, Nat. Photonics **4**, 182 (2010).
3. D. J. Moss, R. Morandotti, A. L. Gaeta, and M. Lipson, Nat. Photonics **7**, 597 (2013).
4. J. Zhu, S. K. Ozdemir, Y. F. Xiao, L. Li, L. He, D. R. Chen, and L. Yang, Nat. Photonics **4**, 46 (2010).
5. Y. Painchaud, M. Aubé, G. Brochu, and M.-J. Picard, in *Bragg Gratings, Photosensitivity, and Poling in Glass Waveguides* (Optical Society of America, 2010), paper BTuC3.
6. I. S. Grudinin, V. S. Ilchenko, and L. Maleki, Phys. Rev. A **74**, 063806 (2006).
7. T. Niemi, M. Uusimaa, and H. Ludvigsen, IEEE Photon. Technol. Lett. **13**, 1334 (2001).
8. G. D. VanWiggeren, A. R. Motamedi, and D. M. Baney, IEEE Photon. Technol. Lett. **15**, 263 (2003).
9. J. E. Román, M. Y. Frankel, and R. D. Esman, Opt. Lett. **23**, 939 (1998).
10. Z. Z. Tang, S. L. Pan, and J. P. Yao, Opt. Express **20**, 6555 (2012).
11. M. Xue, S. L. Pan, X. W. Gu, and Y. J. Zhao, J. Opt. Soc. Am. B **30**, 928 (2013).
12. M. Xue, S. Pan, and Y. Zhao, Opt. Lett. **39**, 3595 (2014).
13. W. Li, W. T. Wang, L. X. Wang, and N. H. Zhu, IEEE Photon. J. **6**, 1 (2014).
14. Z. Z. Tang and S. L. Pan, in *IEEE Topical Meeting on Microwave Photonics* (IEEE 2013), paper W4–27.